Overview on Optical Sensing Techniques Over Deployed Telecom Networks

Overview on Optical Sensing Techniques over Deployed Telecom Networks

Ann Margareth Rosa Brusin
Politecnico di Torino
DET, Torino, Italy
ann.rosabrusin@polito.it

Giuseppe Rizzelli
Politecnico di Torino
DET, Torino, Italy
giuseppe.rizzelli@polito.it

Saverio Pellegrini
Politecnico di Torino
DET, Torino, Italy
saverio.pellegrini@polito.it

Valter Ferrero
Politecnico di Torino
DET, Torino, Italy
valter.ferrero@polito.it

Gabriella Bosco
Politecnico di Torino
DET, Torino, Italy
gabriella.bosco@polito.it

Dario Pilori
Politecnico di Torino
DET, Torino, Italy
dario.pilori@polito.it

Paola Parolari
Politecnico di Milano
DEIB, Milano, Italy
paola.parolari@polimi.it

Pierpaolo Boffi
Politecnico di Milano
DEIB, Milano, Italy
pierpaolo.boffi@polimi.it

Roberto Gaudino
Politecnico di Torino
DET, Torino, Italy
roberto.gaudino@polito.it

***Abstract*—We review in this paper the latest advancements in optical sensing techniques specifically designed for deployment over existing telco fiber networks. Specifically, we focus on sensing techniques that enable coexistence with telecom traffic in Wavelength Division Multiplexing (WDM) optical systems, while allowing fast processing suitable for real time warning/alarm generation using the telemetry systems of modern optical fiber networks. For the most promising solutions, we present physical layer simulations to explore and elaborate on the coexistence constraints, providing a detailed analysis of their feasibility and performance.**

***Index Terms*—Telcommunication networks, fiber sensing.**

I. Introduction

Distributed fiber optical sensing (DFOS) is established in fields like oil and gas pipeline monitoring, but it uses dedicated fibers and specific installation procedures [1]. Recently, several research groups [2]–[5] have demonstrated innovative methods that leverage existing telecom fibers for DFOS. Moreover, in telco WDM optical networks, it is potentially possible to combine DFOS and data by allocating different portions of the optical spectrum for each. This option could in the near future enable widespread and geographically distributed monitoring, with applications including earthquake detection, early warnings of fiber cuts, and monitoring of various other potential hazards near deployed optical fibers.

In this paper, we present a classification and analysis of the most promising DFOS solutions, and then analyze their physical layer compatibility with data on the same fiber. The paper is structured as follows. In Sec. II we introduce a taxonomy of different DFOS solutions and provide preliminary considerations on their compatibility with data transmission, focusing on spectral occupation and mutual nonlinear interference. Secs. III and IV present the results of physical layer simulations that assess the compatibility between sensing and telco data transmission using interferometric sensing (Int-S) and distributed acoustic sensing (DAS), respectively. Finally, conclusions are drawn in Sec. V.

A. M. Rosa Brusin, G. Bosco and P. Boffi are sponsored by the European Union under the Italian National Recovery and Resilience Plan (NRRP) of NextGenerationEU, partnership on 'Telecommunications of the Future' (PE00000001 - program 'RESTART'). G. Rizzelli, V. Ferrero, S. Pellegrini, P. Parolari and R. Gaudino are sponsored by the SURENET project – funded by European Union – Next Generation EU within the PRIN 2022 program (D.D. 104 - 02/02/2022 Ministero dell'Università e della Ricerca). This manuscript reflects only the authors' views and opinions and the Ministry cannot be considered responsible for them.

II. Classification of Optical Sensing Techniques for Deployed Telecom Fiber Networks

To evaluate the PROs and CONs of various DFOS technologies, Table I provides an overview detailing their primary characteristics and compatibility with WDM traffic [6]. In the following analysis, we specifically address two critical factors influencing coexistence feasibility: the DFOS optical bandwidth requirements and the Kerr-induced nonlinear crosstalk between the DFOS and telecom wavelengths.

Raman-based solutions rely on detecting the anti-Stokes induced signal, which is spaced about 13 THz from the pulsed pump. For coexistence with telecom data, precise positioning of the signal wavelength within the WDM spectrum is essential. The placement must avoid proximity to the (usually very strong) pump, due to the nonlinear Raman and/or Kerr effect and ensure sufficient separation from the weak anti-Stokes sensing signal. The only option is using two distinct optical bands, such as the C-band for Raman sensing and the O-band for data transmission (or vice versa).

Brillouin-based and DAS solutions require relatively narrow optical bandwidths for sensing, generally less than the typical 50-100 GHz spacing used for DWDM data transmission. However, fiber Kerr nonlinear effects, caused by high peak power pulses from the sensing system, can limit physical layer compatibility, as discussed in Section IV.

Int-S solutions require minimal optical bandwidth, as the sensing laser is typically not modulated. Additionally, next section simulations demonstrate that these solutions are not affected by Kerr-induced nonlinear cross-talk at the power lev-

	RAMAN sensing	BRILLOUIN sensing	Distributed acoustic sensing (DAS)	Ultra-stable laser interferometry	In-cable Michelson interferometry	State of Polarization in coherent transceivers
Required Back-propagation	YES	YES	YES	YES or loop scheme	YES or loop scheme	NO
Typical response time	Slow (tens of seconds)	Slow (tens of seconds)	Fast (milliseconds)	Fast (microseconds)	Fast (microseconds)	Fast (microseconds)
Max distance	Tens of km	Tens of km	Up to 100 km	Thousands of km	Tens of km	Thousands of km
Spatial resolution	1 m	< 1 m	0.1 m	Requested multiple detection for localization	Requested multiple detection for localization	NO spatial resolution
Temperature measurement	YES	YES	Not used	Not used	Not used	Not used
Strain measurement	Not used	YES	YES	YES	YES	Yes, but only qualitative
Typical power for the optical source	2 W peak	500 mW peak	1 W peak	100 mW CW	10 mW CW	Tens of mW (CW, not pulsed)
Laser linewidth	∼MHz	∼MHz	∼kHz	∼Hz	∼MHz	∼100 kHz
Required Optical bandwidth	f_{laser}±13 THz	f_{laser}±11 GHz	(in principle) Same as laser linewidth	(in principle) Same as laser linewidth	(in principle) Same as laser linewidth	Same as PM-QAM transmission
Compatibility with DWDM on deployed optical networks	NO - Required spectrum and power are too large Different spectral bands are required	In principle, these sensing solutions are spectrally compatible with telco fiber transmission (they use an optical bandwidth equal or smaller than the DWDM channel one) Brillouin and DAS require very high peak power, so that the actual compatibility in terms of signal crosstalk is anyway to be carefully studied case by case		Interferometry usually requires lower power and it has already been demonstrated to have negligible impact on DWDM traffic		Fully compliant

TABLE I
A comparison of possible sensing techniques over deployed optical fiber network.

els of interest, allowing straightforward coexistence between data and sensing λs [7]–[9].

Table I also presents an alternative solution that monitors the state of polarization (SOP) using internal DSP information in coherent receivers [10]. This method is fully compatible with data transmission since the modulated data signal serves dual purposes, eliminating the need for an additional sensing signal. However, unlike the other solutions, it cannot localize anomalous events in the fiber, as it relies on length-integrated time-variations of the SOP.

The following two sections analyze in more details the compatibility of Int-S and DAS sensing signals with data traffic in WDM systems, focusing on Kerr-induced crosstalk. For both solutions, we consider a single span scenario, like in case of non-amplified systems or links between two amplifiers. The analysis is performed through time-domain simulations exploiting the split-step Fourier method (SSFM) [11], that allows to solve the coupled nonlinear Schrödinger equations.

III. Physical-Layer Compatibility for Interferometric Solutions

In this section, we study data and sensing signals coexistence on the same fiber, focusing on nonlinear Kerr crosstalk that may affect the physical layer compatibility. We refer to the setup considered in [6], where 11 WDM channels in the ITU-T DWDM grid centered at 193.4 THz are transmitted over a 100-km span of G.652 SMF fiber. The SMF parameters are: attenuation α=0.2 dB/km, Kerr nonlinearity γ=1.3 1/W/km, chromatic dispersion D=+17 ps/nm/km and PMD=0.05 ps/$\sqrt{\text{km}}$. We simulated two WDM channel spacings, Δf of 50 GHz or 100 GHz. The sensing signal, generated by a CW laser with 100 kHz Lorentzian linewidth, is placed at the center of the WDM comb (channel slot 6).

For data, we assume PM-16QAM at two rates, R_s of 32 Gbaud and 64 Gbaud, and square-root-raised cosine with 0.15 roll-off. At the fiber end, we assume an EDFA with noise figure 5 dB and gain 20 dB to fully recover the propagation loss. Finally, an additive white Gaussian noise (AWGN) source is introduced to reach a given optical signal-to-noise-ratio (OSNR). For instance, to get a pre-FEC bit error rate (BER) of $\simeq 10^{-2}$, the OSNR is set to 14.3 dB. At the receiver side, a WDM DEMUX is used to separate the channels.

The sensing signal is filtered by a 4^{th}-order Super-Gaussian optical filter with 5 GHz cut-off frequency, then it is directly detected by a photodiode and electrically filtered by a 4^{th}-order Butterworth filter with 5 GHz cut-off frequency. For the data signals, a standard coherent DSP is applied. To asses the performance on both signals, we compute the SNR at the end of the respective DSP chain.

To study the potential cross-talk occurring due to fiber Kerr nonlinearity, we test different transmission (TX) powers for the sensing and data signals power, $P_{\text{CW}}\in$[0,25] dBm and $P_{\text{ch}}\in$[-10,5] dBm, respectively. We simulate three different scenarios: 1) Δf=50 GHz and R_s=32 Gbaud, 2) Δf=100 GHz and R_{s}=32 Gbaud, and 3) Δf=100 GHz and R_s=64 Gbaud.

The impact of the sensing signal on data for P_{ch}=0 dBm is reported in terms of SNR in Fig. 1 for the three scenarios and for three CW laser powers: 15 dBm, 20 dBm and 25 dBm. In general, we can observe that no significant SNR degradation occurs when the channel spacing is 100 GHz, neither when the symbol rate is 64 Gbaud. However, a slight SNR reduction due to cross-phase modulation (XPM) can be noticed on channels

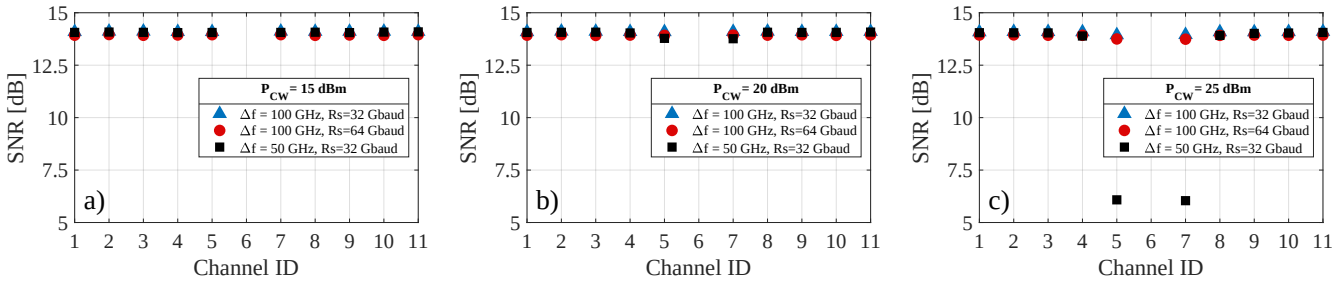

Fig. 1. Int-S solution: signal-to-noise ratio (SNR) of WDM data channels considering P_{ch}=0 dBm power per channel and different CW laser power values: a) P_{CW}=15 dBm, b) P_{CW}=20 dBm and c) P_{CW}=25 dBm. Three different scenarios of channel frequency spacing and symbol rate are reported.

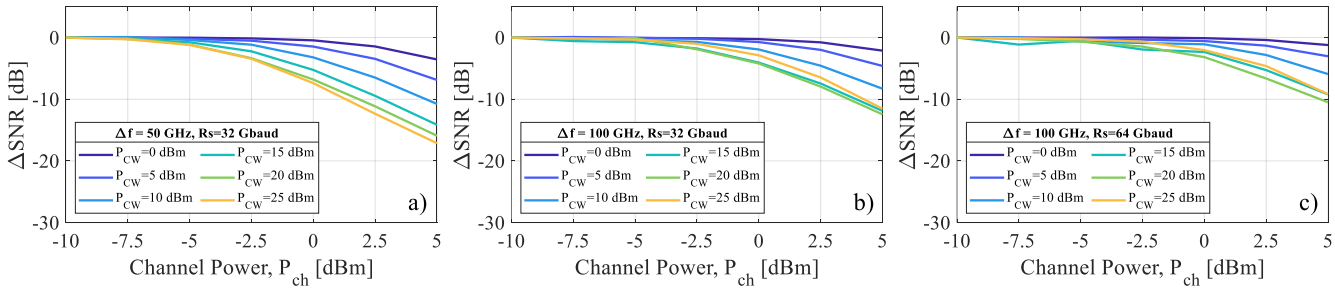

Fig. 2. Int-S solution: ΔSNR for sensing channel as a function of the channel power P_{ch} for different CW laser power P_{CW} for the three scenarios: a) Δf=50 GHz and R_s=32 Gbaud, b) Δf=100 GHz and R_s=32 Gbaud and c) Δf=100 GHz and R_s=64 Gbaud.

5 and 7, the most adjacent to the sensing signal, when the CW laser power is 25 dBm (Fig. 1c)). The impact of XPM becomes stronger when the channels are closer to each other, i.e. when Δf=50 GHz (black square marker), and it starts to become relevant when $P_{\mathrm{CW}} \geq$20 dBm. A dramatic impact is observed on channels 5 and 7 when P_{CW}=25 dBm, for which the SNR decreases to 6 dB.

The effect of data signals on the sensing signal is shown in Fig. 2, which gives the SNR penalty (ΔSNR) as a function of the channel power. Specifically, for each value of P_{CW}, the ΔSNR is given by the SNR normalized with respect to the SNR at P_{ch}=-10 dBm. In general, for all three scenarios, no SNR reduction occurs when the power per channel and the laser power do not reach the highest power levels considered in our simulations. Instead, when P_{ch} and P_{CW} increase, more XPM is generated, thus the ΔSNR decreases. Nevertheless, the impact of the XPM is different depending on the scenario. The strongest SNR reduction is observed when the channels are closer to each other (Fig. 2a)), while less SNR reduction occurs in case of scenario 3 (Fig. 2c)). Interestingly, for Δf=100 GHz, we can notice a saturation effect on the ΔSNR vs P_{ch} curves. This is explained by the stronger nonlinearities generated on the sensing signal that overcome the impact of a higher channel power.

IV. Physical Layer Compatibility for DAS Solutions

In this Section, starting from the experimental setup considered in [6], we investigate on the physical layer compatibility for DAS. This study relies on the simulation setup described in the previous Section, but with the following changes. The fiber span length is now 11.8 km, a typical length for last-mile links, while the power per data channel is P_{ch}=-4 dBm. To emulate DAS, the TX optical pulse is modelled as a Gaussian pulse in time with 50 ns full-width at half-maximum (FWHM) and peak power $P_{\mathrm{DAS}}^{\mathrm{peak}} \in$ [15,24] dBm. Like for the Int-S solution, the OSNR is set at 14.3 dB to have a target BER$\simeq 10^{-2}$, and we analyze three different scenarios of channel frequency spacing and symbol rate.

The DAS pulse induces a non-stationary Kerr crosstalk on the data signal, and thus we needed to evaluated a "time-resolved" SNR, computed over 50 ns time-windows. Fig. 3a) shows results for scenario 1 (Δf=50 GHz and R_s=32 Gbaud) and $P_{\mathrm{DAS}}^{\mathrm{peak}}$=20 dBm for three channels: 7, 9 and 11. Specifically, channel 7 is the closest to the sensing signal, while channel 11 is the farthest. Looking at the evolution of the SNR, although it oscillates around 14 dB, we can observe a slight drop at ~ 3 μs. This drop in the SNR actually occurs when the DAS pulse is present and it is lower for channel 7.

To better understand the phenomenon, we analyze the system intentionally without inserting ASE (OSNR=∞), focusing only on channel 7. Inset i) of Fig. 3a) reports the scattering diagrams resolved over time right after performing adaptive equalization. There, we can see that the SNR drop corresponds to a distortion on the constellation, due to cross-phase modulation (XPM) induced by the sensing signal. However, most of the rotation affecting the constellation is compensated by the carrier phase recovery algorithm, as shown in inset ii) of Fig. 3a).

Since we expect the XPM and the SNR decrease to change with the pulse peak power, in Fig. 3b), we plot the minimum SNR as a function of $P_{\mathrm{DAS}}^{\mathrm{peak}}$ for the three different scenarios. Up to $P_{\mathrm{DAS}}^{\mathrm{peak}}$=19 dBm, there is no significant variation in the SNR, regardless the channel frequency spacing and the symbol

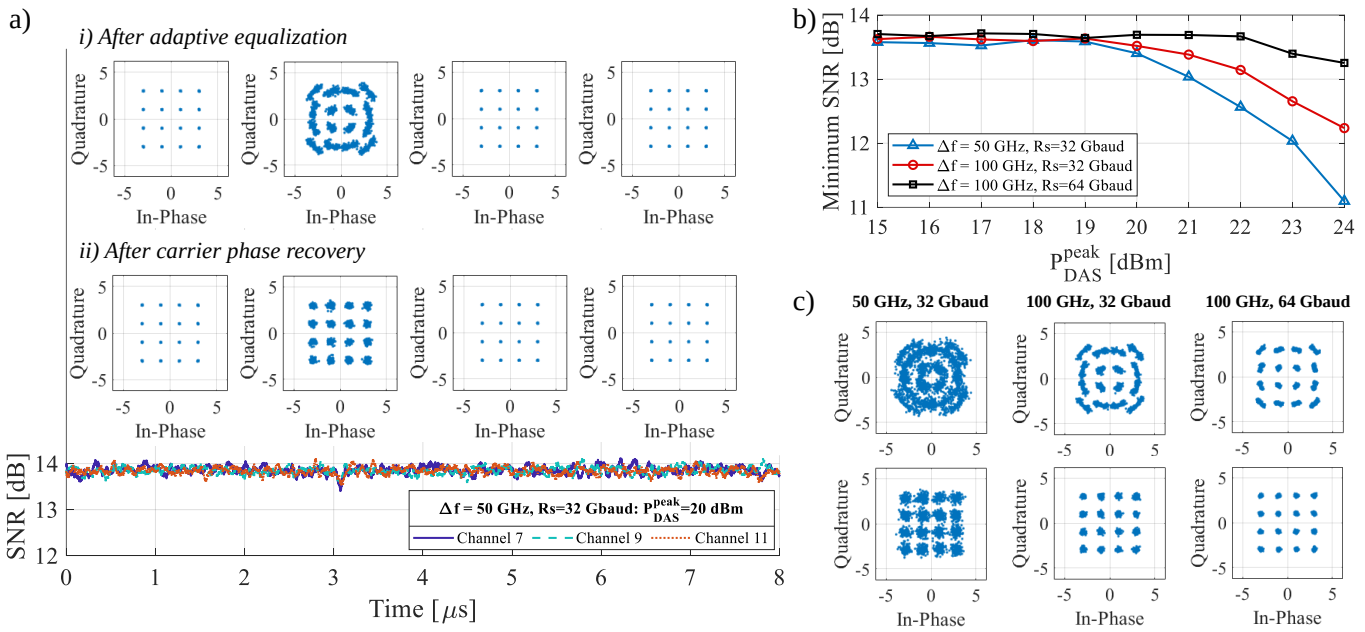

Fig. 3. DAS solution: a) SNR over time for three different data channels in case of *scenario 1* and $P_{\mathrm{DAS}}^{\mathrm{peak}}$=20 dBm. In the insets, the scattering diagrams resolved over time for channel 7 are reported intentionally for OSNR=∞ i) after adaptive equalization and ii) after carrier phase recovery. b) Minimum SNR of channel 7 as a function of the DAS pulse peak power for the three scenarios. c) Scattering diagrams of data channel 7 when the DAS pulse is present for the three scenarios assuming $P_{\mathrm{DAS}}^{\mathrm{peak}}$=23 dBm and OSNR=$\infty$. Top row: after adaptive equalization, bottom row: after carrier phase recovery.

rate. Instead, when the DAS pulse peak power increases, the minimum SNR decreases, meaning that more XPM is generated. This is especially true for scenario 1 (Δf=50 GHz and R_s=32 Gbaud), for which the minimum SNR reduces to 11 dB at $P_{\mathrm{DAS}}^{\mathrm{peak}}$=24 dBm. A smaller reduction of SNR (<1 dB) is observed when Δf=100 GHz, in particular at 64 Gbaud symbol rate.

Qualitatively, the different amount of XPM generated by the sensing signal on the different scenarios can be inferred from the scattering diagrams in Fig. 3c), obtained for channel 7 without ASE (OSNR=∞) and $P_{\mathrm{DAS}}^{\mathrm{peak}}$=23 dBm after adaptive equalization (top row) and after CPR (bottom row). The impact of XPM is stronger when the channels are closer to each other and the symbol rate is smaller. Although CPR is applied, the constellation clouds are quite spread, causing a significant reduction of the SNR. On the other hand, a very limited effect is observed for scenario 3 (Δf=100 GHz and R_s=64 Gbaud), that justifies the negligible reduction of the minimum SNR in Fig. 3b).

V. Conclusions

In this paper, we explored the physical layer compatibility between data and optical sensing techniques on the same fiber for Int-S and DAS sensing techniques. For the first case, we found that there are no significant problems in compatibility unless the sensing and data power are extremely high (i.e. outside the typical ranges of interest). For DAS, we preliminary showed that compatibility is possible, but DAS peak power should be kept under reasonable values.

References

[1] A. Lellouch, and B. L. Biondi, "Seismic Applications of Downhole DAS", *Sensors*, vol. 21, no. 9, 2021.

[2] A. Mecozzi et al., "Use of Optical Coherent Detection for Environmental Sensing," *J. Lightw. Technol.*, vol. 41, no. 11, pp. 3350-3357, 2023.

[3] E. Ip, Y. Huang, G. Wellbrock, T. Xia; M.; T. Wang; Y. Aono, "Vibration Detection and Localization Using Modified Digital Coherent Telecom Transponders," *J. Lightw. Technol.*, vol. 40, no. 5, pp. 1472-1482, 2022.

[4] P. Boffi et al., "Real-Time Surveillance of Rail Integrity by the Deployed Telecom Fiber Infrastructure," *IEEE Sensors Journal*, vol. 23, no. 21, pp. 26012-26021, 2023.

[5] S. Pellegrini et al., "Real-Time Demonstration of Anomalous Vibrations Detection in a Metro-like Environment using a SOP-based Algorithm," in *Proc. of Optical Fibers Communications (OFC) Conference*, San Diego, 2024.

[6] A.M. Rosa Brusin et al., "Overview and analysis of optical sensing techniques over deployed telecom networks," 24th International Conference on Transparent Optical Networks (ICTON), Bari, Italy, 2024, pp. 1-4.

[7] I. Di Luch, M. Ferrario, P. Boffi, G. Rizzelli, H. Wang and R. Gaudino, "Demonstration of structural vibration sensing in a deployed PON infrastructure," in *Proc. of European Conference on Optical Communication (ECOC)*, Dublin, Ireland, 2019, pp. 1-3.

[8] I. Di Luch, M. Ferrarlo, G. Rizzelli, R. Gaudino and P. Boffi, "Vibration Sensing for Deployed Metropolitan Fiber Infrastructures," in *Proc. of Optical Fiber Communications Conference and Exhibition (OFC)*, San Diego, CA, USA, 2020, pp. 1-3.

[9] I. D. Luch, P. Boffi, M. Ferrario, G. Rizzelli, R. Gaudino and M. Martinelli, "Vibration Sensing for Deployed Metropolitan Fiber Infrastructure," *J. of Lightwave Technol.*, vol. 39, no. 4, pp. 1204-1211, 2021.

[10] S. Pellegrini et al., "Estimation Accuracy of Polarization State from Coherent Receivers for Sensing Applications," in *Proc. of 2023 IEEE Photonics Conference (IPC)*, Orlando, FL, USA, 2023, pp. 1-2.

[11] D. Pilori, M. Cantono, A. Carena and V. Curri, "FFSS: The fast fiber simulator software," 2017 19th International Conference on Transparent Optical Networks (ICTON), Girona, Spain, 2017, pp. 1-4.

[12] R. Dar, M. Feder, A. Mecozzi and M. Shtaif, "Pulse Collision Picture of Inter-Channel Nonlinear Interference in Fiber-Optic Communications," *J. Lightw. Technol.*, vol. 34, no. 2, pp. 593-607, 2016.